doi:10.1093/brain/awx208 BRAIN 2017: 140; 2722–2736 | 2722

BRAIN
A JOURNAL OF NEUROLOGY

A ventral glomerular deficit in Parkinson's disease revealed by whole olfactory bulb reconstruction

Bolek Zapiec,[1] Birger V. Dieriks,[2] Sheryl Tan,[1,2] Richard L. M. Faull,[2] Peter Mombaerts[1] and Maurice A. Curtis[2]

Olfactory dysfunction is common in Parkinson's disease and is an early symptom, but its pathogenesis remains poorly understood. Hindering progress in our mechanistic understanding of olfactory dysfunction in Parkinson's disease is the paucity of literature about the human olfactory bulb, both from normal and Parkinson's disease cases. Qualitatively it is well established that the neat arrangement of the glomerular array seen in the mouse olfactory bulb is missing in humans. But rigorous quantitative approaches to describe and compare the thousands of glomeruli in the human olfactory bulb are not available. Here we report a quantitative approach to describe the glomerular component of the human olfactory bulb, and its application to draw statistical comparisons between olfactory bulbs from normal and Parkinson's disease cases. We subjected horizontal 10 μm sections of olfactory bulbs from six normal and five Parkinson's disease cases to fluorescence immunohistochemistry with antibodies against vesicular glutamate transporter-2 and neural cell adhesion molecule. We scanned the immunostained sections with a fluorescence slide scanner, segmented the glomeruli, and generated 3D reconstructions of whole olfactory bulbs. We document the occurrence of atypical glomerular morphologies and glomerular-like structures deep in the olfactory bulb, both in normal and Parkinson's disease cases. We define a novel and objective parameter: the global glomerular voxel volume, which is the total volume of all voxels that are classified immunohistochemically as glomerular. We find that the global glomerular voxel volume in Parkinson's disease cases is half that of normal cases. The distribution of glomerular voxels along the dorsal-ventral dimension of the olfactory bulb in these series of horizontal sections is significantly altered in Parkinson's disease cases: whereas most glomerular voxels reside within the ventral half of olfactory bulbs from normal cases, glomerular voxels are more evenly spread among the ventral and dorsal halves of olfactory bulbs from Parkinson's disease cases. These quantitative whole-olfactory bulb analyses indicate a predominantly ventral deficit in the glomerular component in Parkinson's disease, consistent with the olfactory vector hypothesis for the pathogenesis of this neurodegenerative disease. The distribution of serine 129-phosphorylated α-synuclein immunoreactive voxels correlates with that of glomerular voxels. The higher the serine 129-phosphorylated α-synuclein load of an olfactory bulb from a Parkinson's disease case, the lower the global glomerular voxel volume. Our rigorous quantitative approach to the whole olfactory bulb will help understand the anatomy and histology of the normal human olfactory bulb and its pathological alterations in Parkinson's disease.

1 Max Planck Research Unit for Neurogenetics, Frankfurt, Germany
2 Department of Anatomy and Medical Imaging and Centre for Brain Research, Faculty of Medical and Health Science, University of Auckland, Auckland, New Zealand

Correspondence to: Peter Mombaerts,
Max Planck Research Unit for Neurogenetics, Max-von-Laue-Strasse 4, D-60438 Frankfurt, Germany
E-mail: peter.mombaerts@gen.mpg.de

Keywords: olfaction; glomerulus; VGLUT2; synuclein; voxel

Abbreviations: GGVV = global glomerular voxel volume; NCAM = neural cell adhesion molecule; OSN = olfactory sensory neuron; VGLUT2 = vesicular glutamate transporter 2

Received April 14, 2017. Revised June 20, 2017. Accepted July 8, 2017. Advance Access publication September 3, 2017

Introduction

The human olfactory mucosa is located in the superior aspect of the nasal cavity, just below the cribriform plate, on the nasal septum and on the turbinates (Fig. 1A) (Leopold *et al.*, 2000). Mature olfactory sensory neurons (OSNs) extend a single apical dendrite that ends in a ciliated dendritic knob (Morrison and Costanzo, 1990). These bipolar neurons project their axon through the cribriform plate from the nasal to the cranial cavity. Within the olfactory bulb, the OSN axon terminates in one of several thousand structures of condensed neuropil called glomeruli. Immunohistochemical studies of the human olfactory bulb have revealed basic organizational characteristics, including a superficial olfactory nerve layer that feeds axons into glomeruli situated below (Nakashima *et al.*, 1985; Smith *et al.*, 1991; Maresh *et al.*, 2008). Interneuron populations of the human olfactory bulb have thus far undergone only rudimentary analyses (Smith *et al.*, 1993). Despite the overall similarities in the anatomical organization of the olfactory bulb between human and mouse, there are unmistakable differences. The glomerular array, as evaluated in sections of human olfactory bulbs, is not as neatly arranged as in mouse: co-labelling sections of human olfactory bulbs with antibodies against vesicular glutamate transporter 2 (VGLUT2, encoded by *SLC17A6*) and neural cell adhesion molecule (NCAM, encoded by *NCAM1*) revealed a level of complexity not anticipated (Maresh *et al.*, 2008). The mouse has ~3600 glomeruli in an olfactory bulb (Richard *et al.*, 2010) and 1087 expressed odorant receptor genes in its genome (Saraiva *et al.*, 2015); the axons of the population of mouse OSNs that express a given odorant receptor gene coalesce into a few homogeneous glomeruli per olfactory bulb (Mombaerts *et al.*, 1996; Treloar *et al.*, 2002). But with counts of glomeruli in the human olfactory bulb averaging 5568 (Maresh *et al.*, 2008), and ~400 odorant receptor genes in the human genome (Malnic *et al.*, 2004),

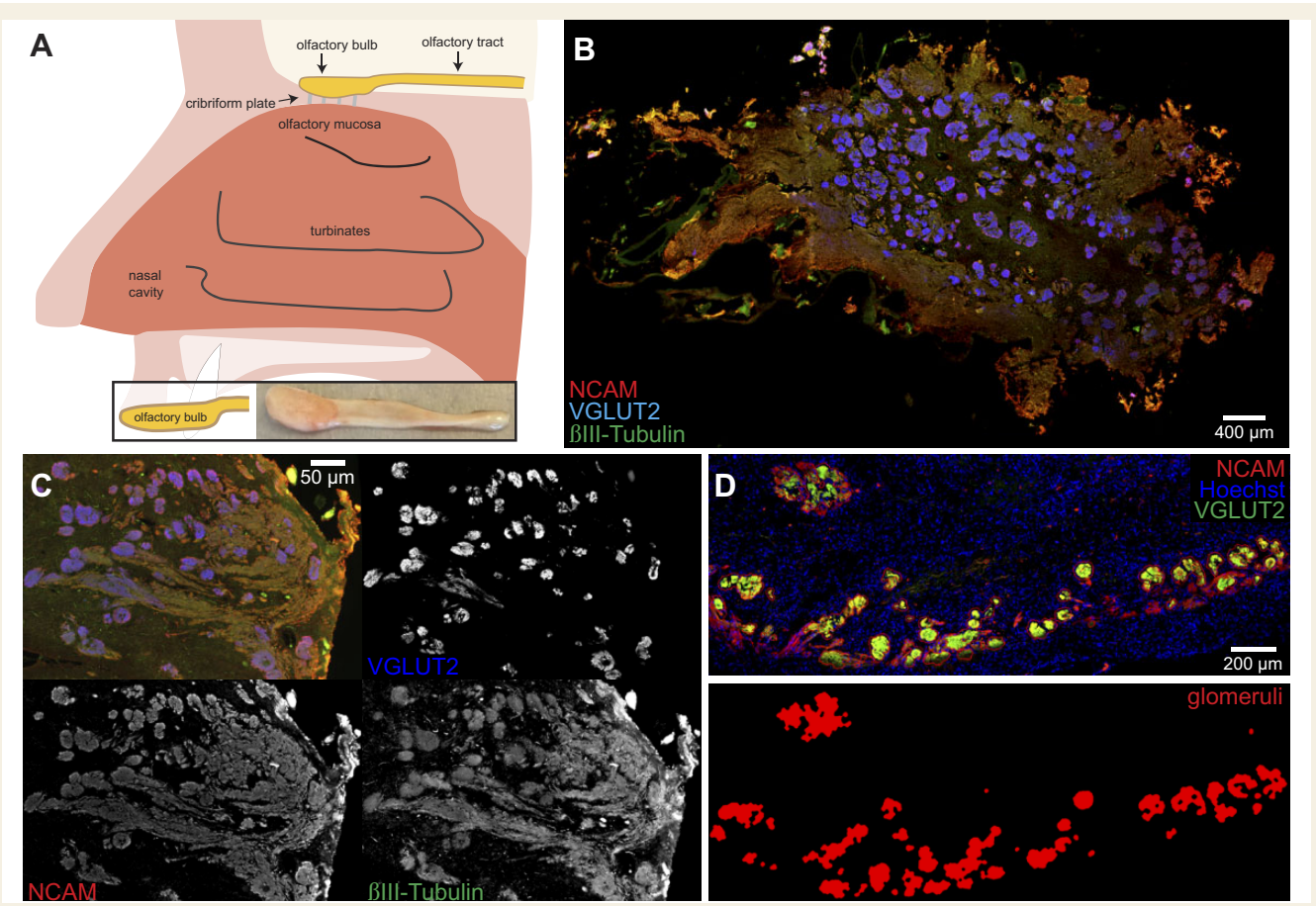

Figure 1 Segmenting glomeruli in scans of horizontal sections of human olfactory bulbs. (**A**) Schematic depicting the olfactory system in a side view of a human head. Dendrites and cell bodies of olfactory sensory neurons reside within the olfactory mucosa in the nasal cavity. Axons of olfactory sensory neurons project through the cribriform plate to the olfactory bulb in the cranial cavity. (**B**) Glomeruli were identified and profiled using a triple-staining protocol with NCAM, VGLUT2, and βIII-tubulin in pilot experiments. The criterion for glomerular identity was co-labelling with all three antibodies. (**C**) The criterion for glomerular identity was reduced to VGLUT2 and NCAM co-labelling in later experiments, after a comparison had revealed that βIII-tubulin signal was redundant with NCAM. The two antibodies are sufficient to identify glomeruli. (**D**) Pipeline of image processing and segmentation used the fluorescent signal to identify glomerular objects for manual verification and correction. The VGLUT2 immunofluorescence signal was used for defining the pixels segmented as glomeruli, which are shown in the *lower* panel.

the ratio of two to three glomeruli per odorant receptor gene does not extend to humans.

The literature on the anatomy and histology of the human olfactory bulb is scant compared to the wealth of knowledge that has been collected about the mouse olfactory bulb. The relevance of a greater understanding of the human olfactory bulb has gained medical relevance in recent years due to the mounting body of evidence for olfactory dysfunction in Parkinson's disease (Ansari and Johnson, 1975; Doty *et al.*, 1988; Doty, 2012) and for initiation of pathology in the olfactory bulb (Braak *et al.*, 2003*a*, 2004; Beach *et al.*, 2009; Adler and Beach, 2016). Olfactory dysfunction has a prevalence of ~90% in early-stage sporadic Parkinson's disease, and is one of the earliest symptoms, typically occurring well before the onset of motor symptoms. The characteristic and diagnostic pathology of Parkinson's disease is the loss of dopaminergic neurons in the substantia nigra pars compacta, accompanied with the accumulation of Lewy bodies and Lewy neurites in this and other regions of the brain. Lewy bodies and Lewy neurites are intraneural inclusions that consist predominantly of fibrils formed by misfolded and aggregated α-synuclein (Spillantini *et al.*, 1997) phosphorylated at residue Ser129 (pSer129) (Fujiwara *et al.*, 2002). Lewy bodies and Lewy neurites are frequently detectable in the olfactory bulb and anterior olfactory nucleus (Daniel and Hawkes, 1992), before they spread to other parts of the brain such as the substantia nigra (Del Tredici *et al.*, 2002; Braak *et al.*, 2003b). The olfactory vector hypothesis (Doty, 2012) proposes that the olfactory system provides a route for xenobiotics (such as viruses, metals, herbicides) to trigger Parkinson's disease. The human olfactory mucosa is directly exposed to the outside air, and OSNs are first-order neurons that project their axons into the brain. The olfactory bulb may also be an entry site for prion-like propagation in other human neurodegenerative diseases (Rey *et al.*, 2017).

Here, we have subjected horizontal 10-µm section series of human olfactory bulbs from six normal cases and five Parkinson's disease cases to fluorescence immunohistochemistry for VGLUT2 and NCAM. We also stained a subset of sections for tyrosine hydroxylase (TH) and for pSer129 α-synuclein. We developed a novel pipeline for image processing, and generated 3D reconstructions of the individual whole olfactory bulbs. To accommodate the absence of a neat arrangement of the glomerular array in the human olfactory bulb, we defined a novel parameter: the global glomerular voxel volume (GGVV), which is the sum of the volume of all voxels that are classified immunohistochemically as glomerular. We found that the higher the load of pSer129 α-synuclein, the lower the GGVV, suggesting a causal relationship. Our analyses reveal a predominantly ventral deficit in the glomerular component in Parkinson's disease. This finding is consistent with the olfactory vector hypothesis for the pathogenesis of this neurodegenerative disease.

Materials and methods

Tissue acquisition

Post-mortem human olfactory bulbs were procured from the Neurological Foundation Douglas Human Brain Bank at the Centre for Brain Research, University of Auckland, New Zealand. Informed consent of the family was obtained prior to autopsy. The University of Auckland Human Participants Ethics Committee approved the protocols (Ref: 011654). The normal olfactory bulbs were from cases that had no known clinical history of neurological disease and no apparent pathological abnormalities upon examination. The Parkinson's disease cases had a disease duration ranging from 9 to 20 years, with an average of 13.2 years (Table 1). Pathological examination by a neuropathologist revealed Lewy bodies in the substantia nigra and frontal lobe, and pigment incontinence and cell loss in the substantia nigra, confirming the diagnosis of Parkinson's disease.

Tissue collection and preparation

Upon arrival at the Human Brain Bank, specimens were fixed with 15% formaldehyde in 0.1 M phosphate buffer for 24 h at room temperature. Olfactory bulbs that passed a visual quality control for gross morphology were dehydrated in a graded ethanol series, and embedded in paraffin wax using a Leica Tissue Processor. Dehydration comprised sequential steps of 70%, 80%, 2 × 95%, and 3 × 100% ethanol for 20 min each at room temperature. Next the tissue was cleared in xylene, 2 × 30 min, and impregnated with molten paraffin wax during three cycles of 25 min each. Paraffin blocks with embedded olfactory bulbs were cooled to 4°C and sectioned horizontally at a thickness of 10 µm on a rotary microtome (Leica Biosystems, RM2235). Cut sections were floated in a waterbath set at 37–39°C (Leica Biosystems, HI1210), mounted individually on Superfrost™ Plus slides (Menzel-Gläser), and air-dried for 18 h at room temperature.

Immunohistochemistry

Slides were heated to 60°C for 1 h to melt the paraffin wax. Slides were cleared in xylene (2 × 1 h at 60°C), and rehydrated in an ethanol series: 2 × 100% (10 min), 1 × 95% (10 min), 1 × 80% (5 min) and 1 × 75% ethanol (5 min) followed by 3 × distilled H_2O (5 min). Heat-induced epitope retrieval was performed with a Tris-EDTA (pH 9.0) buffer in a pressure cooker (2100 Antigen Retriever, Aptum Biologics Ltd.) for 2 h at 121°C. Following cooling, slides were washed for 5 min in phosphate-buffered saline (PBS) and permeabilized twice in PBST (0.2% Triton™ X-100 in PBS) for 5 min each. The slides were blocked for 1 h in 10% normal donkey serum (Millipore #S30) or 10% normal goat serum (Gibco #16210-072). Primary antibodies were diluted in PBST, and the slides were incubated for 24–72 h at 4°C in a humidified chamber. Slides were washed once in PBST and twice in PBS for 5 min each. Secondary antibodies were diluted to 1:1000 (donkey antibodies) or 1:400 (goat antibodies), and the solution was placed on the slides for 3 h at room temperature. Slides were washed for 5 min in PBS, and then submerged for 5 min in PBS containing a 1:20 000 dilution of Hoechst 33342 (Molecular

Table 1 Case information

Case	Gender	Age	Cause of death	Post-mortem delay, h	Pathology	Duration of Parkinson's disease, years
OFB41	M	83	Left ventricular failure	21		
OFB42	M	83	Ischaemic heart disease	18		
OFB43	F	68	Hypertensive heart disease	22		
OFB48	M	72	Ischaemic heart disease with secondary coronary heart disease	34		
OFB58	M	60	Suicide, asphyxia	17–36		
OFB59	M	67	Complications of surgery, internal bleeding	20		
PD30	M	82	Multiple organ failure	19	Parkinson's disease with diffuse cortical Lewy body disease	11
PD42	M	84	Myocardial infarction	21	Parkinson's disease	14
PD50	M	88	Myocardial infarction, ischaemic heart disease	6	Parkinson's disease with cortical Lewy bodies in cingulate gyrus	20
PD52	M	54	Acute myocardial infarction	5	Diffuse Lewy body disease, idiopathic Parkinson's disease and cortical Lewy body disease	12
PD53	F	79	Renal failure	25	Idiopathic Parkinson's disease and probable early cortical Lewy body disease	9

Probes # H1399) to counterstain nuclei, then for 5 min in PBS. Slides were coverslipped with ProLong® Gold (Molecular Probes #P36930) and left overnight at room temperature in the dark. Slides were sealed around the edges using nail polish, and stored at 4°C in the dark. Primary antibodies were: guinea pig anti-VGLUT2 (1:1000, Frontier Science #GP-Af670-1), rabbit anti-NCAM (1:000, Santa Cruz Biotechnology #H-300; sc10735), mouse monoclonal anti-β-III tubulin (1:000, Sigma #T8660), mouse monoclonal anti-TH (1:500 or 1:1000, Millipore #MAB5280), and rabbit monoclonal anti-α-synuclein phospho S129 (EP1536Y), which was conjugated with biotin (1:2000, Abcam #190628). Secondary antibodies were donkey anti-guinea pig Alexa Fluor® 647 (Jackson ImmunoResearch Laboratories #706-605-148), donkey anti-rabbit Alexa Fluor® 594 (Molecular Probes #A21207), donkey anti-mouse Alexa Fluor® 488 (Molecular Probes #A11029); goat anti-guinea pig Alexa Fluor® 647 (Invitrogen #A21450), goat anti-rabbit Alexa Fluor® 594 (Invitrogen #A11037), goat anti-mouse Alexa Fluor® 488 (Invitrogen #A11029).

For fluorescence quenching and restaining, the coverslips from stained and imaged sections were removed, and slides washed in PBST to remove ProLong® Gold. Sections were placed on ice for 2 × 3 h covered with H_2O_2 quenching solution (3% H_2O_2 pH 9.5), and exposed to light emitted from a light bulb. Sections were washed with PBS and covered with H_2O_2 quenching solution overnight at room temperature. Sections were then washed in PBS, blocked in normal goat serum, immunostained, and biotinylated rabbit anti-α-synuclein phospho S129 was revealed with Streptavidin-Alexa Fluor® 488 (1:400; Invitrogen #S11223).

Case OFB41 was stained for VGLUT2, NCAM, and β-III tubulin using donkey secondary antibodies. Cases OFB43 and PD42 were stained for VGLUT2 and NCAM with complete coverage, and every third slide for TH, all in combination with donkey secondary antibodies. Cases OFB42, OFB48, PD30, and PD50 were stained for VGLUT2, NCAM, and β-III tubulin using donkey secondary antibodies. After scanning the slides, a subset underwent fluorescence quenching and stained for α-synuclein phospho S129-biotin and Streptavidin-Alexa Fluor® 488. Cases OFB58, OFB59, PD52, and PD53 were initially stained at every third section for VGLUT2 and NCAM in combination with donkey secondary antibodies. Another set of unstained slides were stained for VGLUT2, α-synuclein phospho S129, and TH in combination with goat secondary antibodies.

Image processing

The Ethics Council of the Max Planck Society (*Ethikrat der Max-Planck-Gesellschaft*) approved the scanning of the stained sections in the Max Planck Research Unit for Neurogenetics in Frankfurt, Germany. Slides were scanned using a Pannoramic MIDI fluorescence digital slide scanner (3DHISTECH). Images were processed using a custom pipeline that we developed specifically for these studies. Section alignment and 3D visualization of data were performed with Amira software (FEI, Hillsboro, OR, USA). Aligned sections were then processed using a CellProfiler pipeline (Carpenter *et al.*, 2006) programmed to segment VGLUT2-stained glomeruli on olfactory bulb sections. A morph operation was performed to fill in small gaps of signal within glomeruli. Segmented pixels were corrected manually to remove false positives and false negatives using the segmentation toolkit in Amira. Segmented images of sections were subjected to volumetric analyses in Amira or MATLAB.

Spatial analysis of 3D reconstructions of human olfactory bulbs

The dimensions of the human olfactory bulb specimens were ~3 mm in the dorsal-ventral dimension, 5 mm medial-lateral, and 10 mm anterior-posterior. Quantitative analysis of

reconstructed olfactory bulbs was performed on segmented 3D reconstructions that comprised stacks of indexed images. Each pixel was contained within a region of interest defined either as olfactory bulb (automatically segmented from the black pixels surrounding the olfactory bulb and manually separated from the lateral olfactory tract just beyond the most posterior glomerulus), glomerular, TH+, or pSer129 α-synuclein+. As the 10-µm sections were imaged using a widefield fluorescence scanner, each image plane had a thickness of 10 µm. When the images were stacked atop each other, the pixels (~1 µm × 1 µm) resulted in voxels of ~1 µm × 1 µm × 10 µm (= 10 µm^3). Thus, a perfectly spherical glomerulus with a diameter of 60 µm is represented by 11 350 voxels.

Depth analysis was performed by generating a custom multilayer mask for each olfactory bulb, with each layer converging toward the core of the olfactory bulb. The 3D datasets containing glomerular, TH+, or pSer129 α-synuclein+ voxels were then tagged as belonging to one of these layers, and the number of voxels within each layer was quantified, thus binning the voxels according to their depth profiles. Data were visualized with the help of a false-colour look-up table (spanning across blue, green, yellow, and red) that coloured the voxels according to their layer (from superficial to deep). Datasets were normalized to the sum of each category of voxels for an olfactory bulb and to the depth profile along 10 bins spanning from the surface to the core.

For analysis of the spatial distribution of glomerular voxels in the dorsal-ventral dimension, the indexed pixel images were exported in coronal format, with one image per pixel along the anterior–posterior axis perpendicular to the plane of sectioning. A custom MATLAB script processed the exported images of virtual coronal sections of the olfactory bulb. The outline of the olfactory bulb was used to define the midline in both dorsal-ventral and medial-lateral aspects. Each image was divided along these midlines producing four images, one for each quadrant. The quadrants were further bisected diagonally resulting in octants. A coronal virtual section was thus subdivided into eight sectors. Glomerular pixels were quantified for each octant, and the voxel quantities were calculated as mm^3 values for each quadrant or summed to determine the GGVV.

The 3D density heat map analysis was performed on segmented glomerular datasets in Amira. The cluster density tool was used to interrogate the neighbourhood of each glomerular voxel for other glomerular voxels. The output of this analysis indicated how many glomerular voxels were present in a spherical neighbourhood corresponding to a 300-µm radius. The value itself was a count of glomerular voxels within the prescribed radius. The visualization of these data was performed by applying a pseudocolour gradient along the value range of the counts, with the highest density voxels labelled in red, intermediate density in yellow, and lowest density in grey–black.

Statistical analysis

Global glomerular voxel volumes were compared using a two-tailed *t*-test with Welch's correction for unequal variances and sample sizes in GraphPad Prism 5 (GraphPad Software Inc.) resulting in t = 2.464, df = 8, and a *P*-value of 0.0391. The alpha values for significance were set as: $*P \leqslant 0.05$, $**P \leqslant 0.01$, and $***P \leqslant 0.001$. Testing for glomerular voxels in dorsal versus ventral half of the olfactory bulb was also performed using a two-tailed Welch's *t*-test accounting for unequal variances and sample sizes in GraphPad Prism 5, and resulted in t = 5.976, df = 6, and a *P*-value of 0.0010. Pearson correlation coefficients for depth profile analysis were determined using GraphPad Prism 5.

Results

Because of the precious nature of human brain samples, extensive means were taken to obtain the maximum amount of information from the available material. With the goal of comparing the 3D organization of the glomerular array in the olfactory bulbs between normal and Parkinson's disease cases, we first chose an approach based on immunohistochemistry for VGLUT2, NCAM, and β-III tubulin. The staining of the olfactory nerve layer with NCAM and β-III tubulin allowed for the verification of the orientation of the olfactory bulb in the dorsal-ventral dimension, based on the thicker olfactory nerve layer along the ventral aspect. Although VGLUT2 alone can label glomeruli, the imperfect laminar organization of the human olfactory bulb and the high incidence of background antibody staining dictated a conservative approach: only triple labelling by VGLUT2, NCAM, and β-III tubulin would qualify for glomerular classification (Fig. 1B). After pilot experiments, we found that the co-labelling of VGLUT2 and NCAM proved sufficient in defining glomerular structures (Fig. 1C), as was the experience of Maresh *et al.* (2008). Our image processing procedure consisted of aligning scans of horizontal sections using Amira followed by a CellProfiler-based pipeline using image math, a mixture-of-Gaussians thresholding, and object morphing. This procedure permits the segmentation of immunohistochemistry images for 3D reconstruction and analysis (Fig. 1D).

Invasive and atypical glomeruli

Glomeruli located deep within the olfactory bulb disrupt its laminar organization (Fig. 2A). The vast majority of the glomeruli were located directly below the outer nerve layer, within a less organized but still recognizable glomerular layer. Some OSN axon bundles projected deep into the olfactory bulb (as deep as halfway across) and formed numerous glomerular or glomerular-like structures, which we term 'invasive'. Various views of a 3D-reconstructed olfactory bulb from a normal case illustrate the invasive glomeruli (Fig. 2B–F). In addition to the invasive glomeruli, human olfactory bulbs abound in structures that qualify as glomeruli histochemically, but lack many of the typical morphological characteristics seen in the mouse olfactory bulb. These atypical glomerular-like structures include small glomeruli, irregularly shaped glomeruli, and tangles of glomeruli. Invasive glomeruli exhibited a morphology that was intact, round, or of grainy texture akin to canonical glomeruli found in the glomerular layer (Fig. 2G),

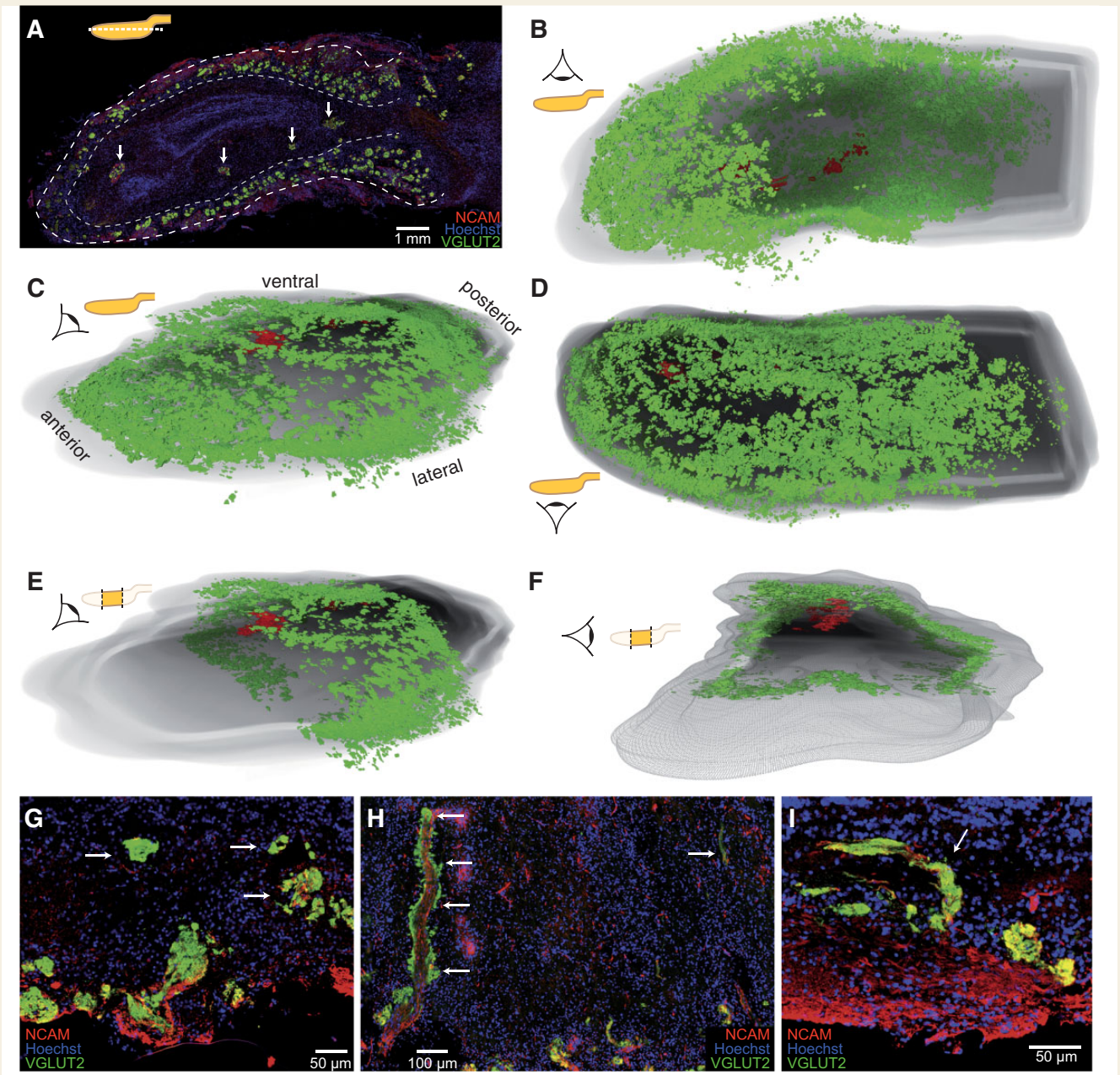

Figure 2 Invasive glomeruli. (**A**) Immunofluorescence of a horizontal section of the olfactory bulb from normal Case OFB42 with antibodies against VGLUT2 and NCAM. Some glomeruli (arrows) protrude well below the inner boundary of the glomerular layer (grey dotted line). The outer boundary of the glomerular layer (white dotted line) is adjacent to the olfactory nerve layer, which is at the surface of the bulb. (**B–F**) 3D reconstruction of normal Case OFB42. Glomerular voxels are rendered in green, and examples of invasive glomeruli in red. A view of the dorsal surface (**B**) demonstrates dense glomerular coverage toward anterior but not posterior. A slightly slanted view (**C**) showing the anterior-ventral-lateral surface provides a view of invasive glomeruli between gaps of superficial glomeruli. A view of the ventral surface (**D**) demonstrates that glomerular coverage extends ventrally much further toward posterior compared to dorsally. By only showing glomerular voxels midway along the anterior-posterior axis (**E**), the deep location of the invasive glomeruli can be fully appreciated when viewed from anterior (**F**). (**G**) Immunofluorescence image from normal Case OFB48 depicting structures (arrows) with the immunohistochemical characteristics and typical morphology of glomeruli, and located outside the glomerular layer. (**H**) Immunofluorescence image from normal Case OFB48 depicting atypical structures such as stalks of axons with small glomeruli (left-facing arrows) and branching patterns or tangles of axons (right-facing arrow). (**I**) Immunofluorescence image from normal Case OFB43 depicting a hybrid structure (arrow), which resembles a conventional glomerulus toward the olfactory nerve layer but resembles a linear tangle toward the external plexiform layer.

consisted of elongated stalks or tangles of comingling axons (Fig. 2H), or were hybrids of a canonical glomerulus and the tangle morphology (Fig. 2I). Glomerular clusters located deep inside the olfactory bulb, well beyond the classical glomerular layer, were found both in normal and Parkinson's disease cases, and varied in abundance.

Quantification of the invasive glomerular component in 3D reconstructions

To quantify the abundance of invasive glomerular voxels, a 2D-based analysis would have been suitable if the human olfactory bulb were spherical. However, because of the oblong and asymmetrical shape of the human olfactory bulb, a glomerulus that appears to be located in the centre of a section may actually reside at short distance from the surface in the *z*-plane. Therefore, we developed a 3D-based analysis. We generated a set of layers that converge from the surface of the olfactory bulb toward the core (Fig. 3A), and assigned a depth to each glomerular voxel on the basis of the layer in which it was located. By using these layers to mask glomerular voxels, we were able to quantify and visualize the glomerular depth characteristics of an olfactory bulb. Glomerular voxels were restricted to the glomerular layer in many olfactory bulbs (Fig. 3B). Some olfactory bulbs had extensive glomerular formations in deeper layers as well (Fig. 3C). By plotting the profile along the depth axis, it is clear that all olfactory bulbs harbour the vast majority of their glomerular voxels near the surface (Fig. 3D). Comparing the normal versus Parkinson's disease cases revealed a trend toward more invasive glomeruli in Parkinson's disease cases (Fig. 3E).

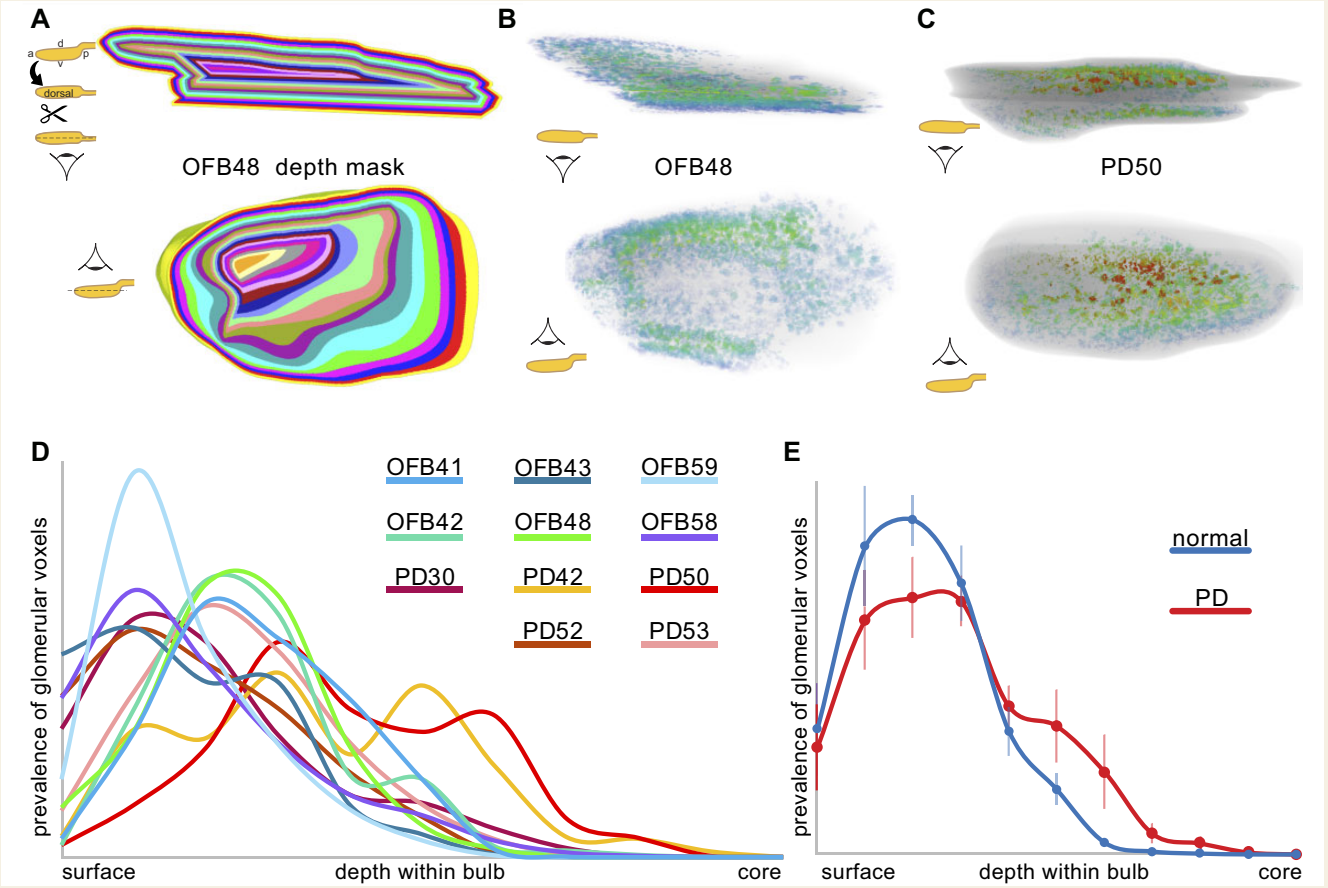

Figure 3 Quantification of invasive glomeruli. (**A**) Cross-section images of a 3D mask with bins defined by the distance of each glomerular voxel from the nearest surface. (*Top*) Lateral view of such a 3D mask that was cut along the anterior-posterior (a–p) and dorsal-ventral (d–v) axes at a point halfway on the medial-lateral axis, representing a sagittal view on a virtually-cleaved olfactory bulb. (*Bottom*) Dorsal view of the 3D mask that was cut along the anterior-posterior and medial-lateral axes halfway along the dorsal-ventral plane, representing a horizontal view on a virtually-cleaved olfactory bulb. (**B** and **C**) 3D rendering of the glomerular voxels from Cases OFB48 and PD50 with a colour gradient indicating the depth of each glomerular voxel. The gradient extends from superficial (blue) to deep (red). The rendering of normal Case OFB48 (**B**) reveals mostly blue and green voxels, indicating that the vast majority of glomerular voxels are near the surface. The high abundance of red voxels in Parkinson's disease Case PD50 (**C**) indicates that there are numerous glomerular voxels deep within the olfactory bulb. (**D**) Plots of the abundance of glomerular voxels along the surface-to-core dimension. The *y*-axis is normalized to be proportional for each olfactory bulb, such that the area below a curve amounts to 100% of the glomerular voxels for a given olfactory bulb. The *x*-axis is normalized to the distance from the surface to the core along 10 bins. The core is defined as the point that is the furthest from all surfaces of the olfactory bulb. (**E**) The profiles in **D** were averaged between the two categories of samples [normal versus Parkinson's disease, (PD)] and plotted. Error bars are standard error of the mean (SEM).

Tyrosine hydroxylase as a presumptive marker for neuronal activation

TH immunoreactivity in the human olfactory bulb is restricted to periglomerular neurons, which are dopaminergic (Smith *et al.*, 1991). In the mouse and rat olfactory bulb, TH immunoreactivity in periglomerular neurons reflects neuronal activation (Baker *et al.*, 1983; Baker, 1990). We labelled a subset of sections with antibodies against TH. Throughout the olfactory bulb, TH+ neurons labelled brightly and surrounded glomeruli (Fig. 4A), as is typical for activated glomeruli in rodents. The proportion of olfactory bulb voxels that are TH+ was on average 14-fold higher in normal cases than in Parkinson's disease cases

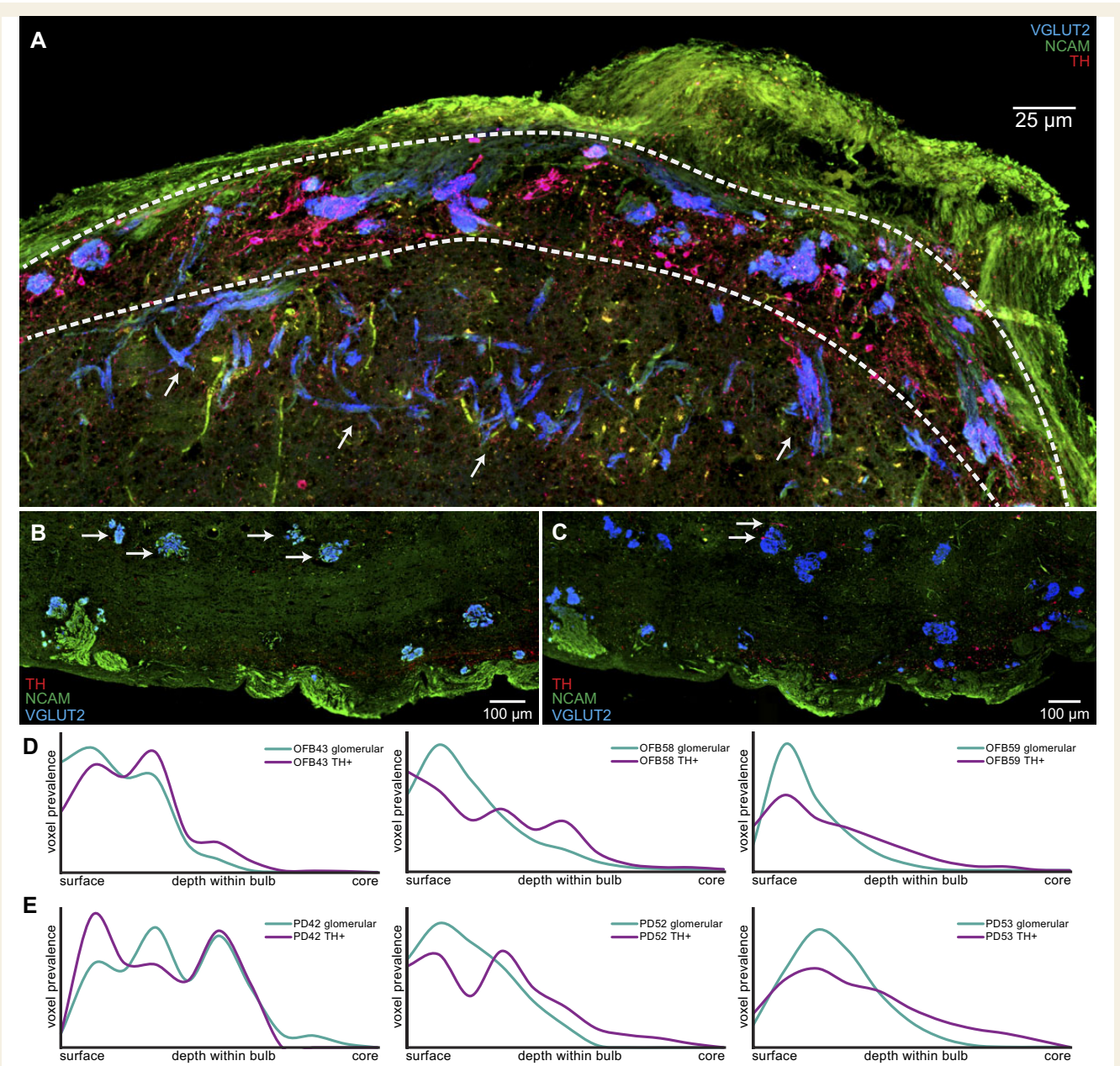

Figure 4 Olfactory bulb neurons immunoreactive for TH. (**A**) Immunofluorescence for TH shows robust staining along the glomerular layer (area between dotted lines) from normal Case OFB43. Glomeruli with the appearance of tangles of axons (arrows) are often located in areas corresponding to the external plexiform layer. (**B**) Clusters of glomeruli deep in the olfactory bulb from Parkinson's disease Case PD42, well beyond the glomerular layer, lack TH+ neuronal somata in the vicinity of glomeruli (arrows). (**C**) TH+ neuronal somata (arrows) from Parkinson's disease Case PD42 are occasionally present in the vicinity of invasive glomeruli. (**D** and **E**) Depth profiles comparing the distribution of TH immunoreactive voxels versus that of glomerular voxels for six olfactory bulbs, three from normal cases (**D**) and three from Parkinson's disease cases (**E**). The majority of the TH immunoreactive signal is detected near the surface, with a similar distribution pattern as glomeruli. Deep glomeruli also correlate with deeper TH profiles.

(n = 3 cases each). In sharp contrast to the glomeruli located superficially within the glomerular layer, the glomeruli located deep within the bulb appeared to be mostly devoid of TH+ somata in their vicinity (Fig. 4B), further differentiating them from the classical features of glomeruli in rodents. There was TH immunoreactivity within and around some deep glomeruli, reflecting most likely the dendritic processes of TH+ neurons, and in rare instances TH+ somata (Fig. 4C). Indeed, when profiling for TH immunoreactivity using a similar signal depth assay as used on glomeruli, TH+ voxels exhibited distributions across the 10 depth bins that mirror those of glomerular voxels, both in normal cases (Fig. 4D) and in Parkinson's disease cases (Fig. 4E). The relationship between glomerular voxels and TH+ voxels was direct and significant in all cases (Pearson correlation: Case OFB43, r = 0.9133, P = 0.0002, R^2 = 0.8341; Case OFB58, r = 0.8415, P = 0.0023, R^2 = 0.7081; Case OFB59, r = 0.9182, P = 0.0002, R^2 = 0.8430; Case PD42, r = 0.9072, P = 0.0003, R^2 = 0.8229; Case PD52, r = 0.8733, P = 0.0010, R^2 = 0.7627; Case PD53, r = 0.9623, $P < 0.0001$, R^2 = 0.9261). Thus, it appears that deep glomeruli are innervated by TH+ neurons and may be activated by olfactory stimuli.

Global glomerular voxel volume

Next, we sought to define a parameter to quantify the volume of all glomeruli and glomerular-like structures in a human olfactory bulb. In a first set of experiments, we used seven olfactory bulbs: four normal cases (Cases OFB41, OFB42, OFB43, and OFB48) and three Parkinson's disease cases (Cases PD30, PD42, and PD50) (Table 1). After staining, scanning, and image processing, we examined the segmentation manually to correct for false-positive or false-negative segmentation resulting from staining irregularities. These corrected datasets were reconstructed in 3D, enabling the visualization of glomerular voxels (Fig. 5A and B). We define the GGVV for a given olfactory bulb as the sum of the volumes of all glomerular voxels. The range in GGVV among these four normal cases was between 0.36 and 1.22 mm^3. In contrast, the three Parkinson's disease cases had a GGVV between 0.20 and 0.42 mm^3. Based on modelling using datasets from the first set of experiments containing every section spanning an olfactory bulb, the expected error in determining GGVV at a sampling of one out of three sections would be only ~2%. Therefore, for the second set of four olfactory bulbs (Cases OFB58, OFB59, PD52, and PD53; Table 1), we processed every third section. By quantifying the segmented glomerular voxels of both experimental series, we found that the average GGVV of Parkinson's disease cases (0.395 ± 0.248 mm^3) is ~47% that of normal cases (0.840 ± 0.35 mm^3) (Fig. 5C).

Glomerular distribution in normal and Parkinson's disease cases

Next, we developed an automated analysis pipeline to quantify the abundance of glomerular voxels in various regions of the olfactory bulb. From the 3D reconstructions we generated sets of virtual coronal sections that span the entire anterior–posterior length of the olfactory bulb. We

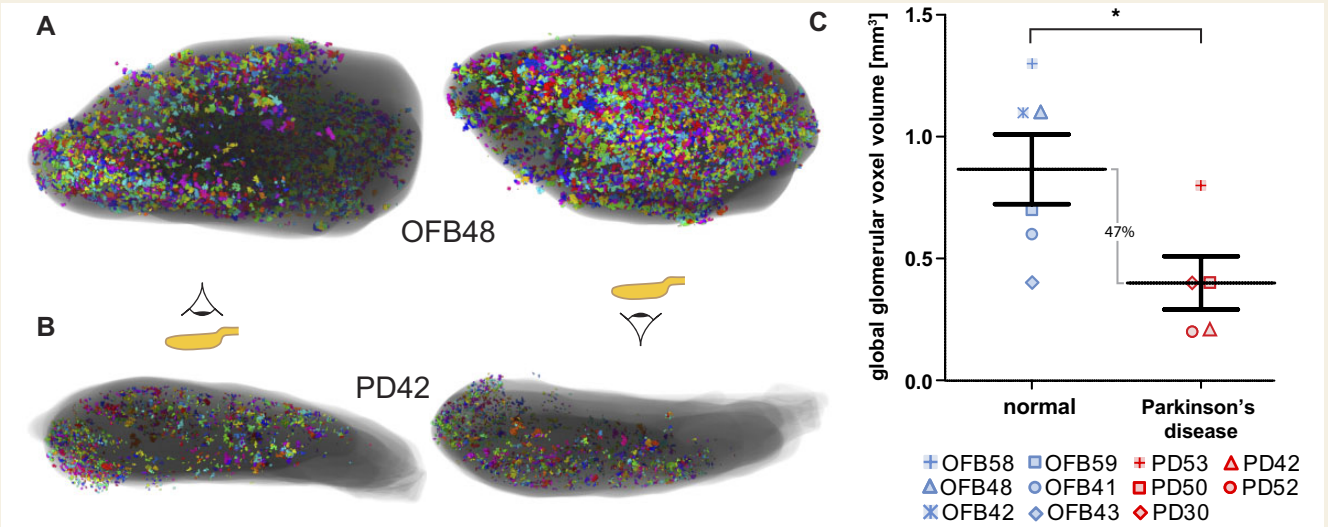

Figure 5 Profiling glomeruli in normal and Parkinson's disease cases. 3D reconstructions from section series spanning entire olfactory bulbs from normal and Parkinson's disease cases. Individual glomeruli are labelled in confetti-like colours. (**A**) The surface of normal Case OFB48 is densely permeated with glomerular voxels, both dorsally and ventrally. Glomerular voxels on the dorsal surface are restricted toward anterior (*left*). The ventral aspect exhibits a high density of glomerular voxels from anterior to posterior (from *left* to *right*). (**B**) The glomerular voxels in Parkinson's disease Case PD42 are relatively sparse, with comparable density and incidence along the dorsal and ventral surfaces on the bulb. (**C**) The GGVV in mm^3 was calculated by summing all segmented glomerular voxels. Horizontal line indicates mean, bars indicate SEM; two-tailed t-test P = 0.0391.

then divided each of these virtual sections into eight sectors or octants, and quantified the abundance of glomerular voxels in each sector (Fig. 6A). A graph plotting the GGVV versus the percentage of glomerular voxels within the dorsal or ventral half of the olfactory bulb demonstrates the divergent characteristics of these three groups (Fig. 6B). With the notable exception of Case PD53, the Parkinson's disease cases have a smaller GGVV than most

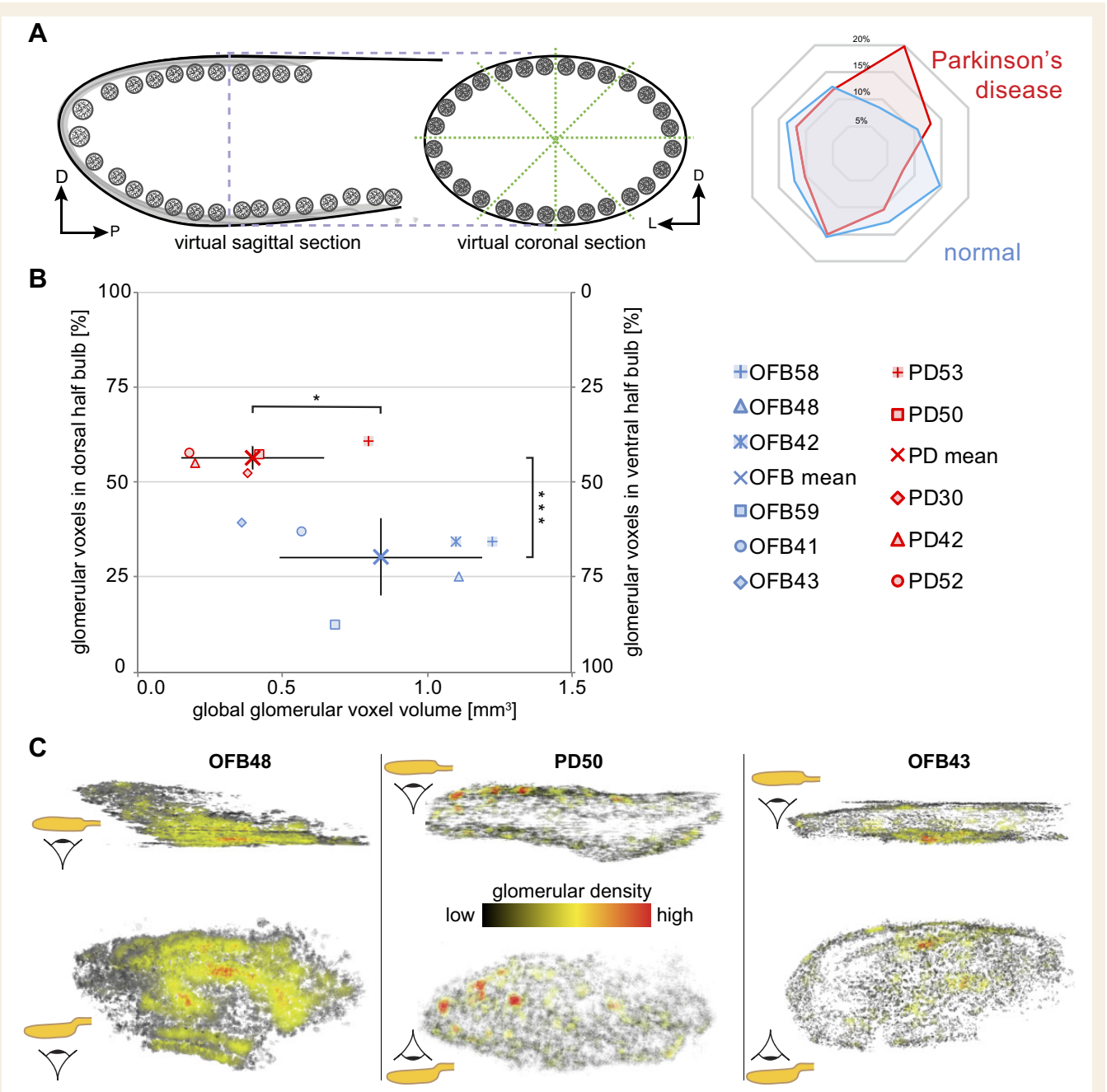

Figure 6 Distribution of glomerular voxels in normal and Parkinson's disease cases. (**A**) Segmented 3D datasets of olfactory bulbs were converted into virtual coronal sections. The coronal sections were subdivided into eight segments, and the fraction of glomerular voxels within each segment was computed. The two groups (Parkinson's disease and normal) show a differential distribution of glomeruli among these octants (n = 11 olfactory bulbs). (**B**) Plotting the percentage of glomerular voxels in the ventral and dorsal halves of the olfactory bulb against the GGVV shows significant differences between Parkinson's disease cases (red) and normal cases (blue). (**C**) Density heat maps visualize the density of glomerular voxels on the 3D reconstruction of an olfactory bulb, by pseudocolouring each glomerular voxel according to how many glomerular voxels are found within a 300-µm radius. Normal Case OFB48 is densely covered with glomerular voxels ventrally but has few glomerular voxels dorsally. Parkinson's disease Case PD50 has a few hotspots dorsally, and overall glomerular voxels are more evenly distributed compared to in Case OFB48. Normal Case OFB43 has many glomerular voxels ventrally, but few on the sides and is less densely covered dorsally.

normal cases. In normal cases, there is a ventral preponderance of glomerular voxels, with 0.255 ± 0.132 mm^3 (~30%) in the dorsal half and 0.585 ± 0.249 mm^3 (~70%) in the ventral half. But glomerular voxels in the Parkinson's disease cases are more evenly distributed along the dorsal-ventral dimension, with the dorsal half containing 0.223 ± 0.154 mm^3 (~56%) of the glomerular voxels and 0.172 ± 0.094 mm^3 (~44%) for the ventral half. There is thus a glomerular voxel reduction of 0.032 mm^3 (~13%) in the dorsal half, and of 0.413 mm^3 (~71%) in the ventral half.

Finally, we visualized the distribution of glomerular voxels directly by applying a glomerular density heat map. This visualization (Fig. 6C) pseudocolours each glomerular voxel according to the number of glomerular voxels located in a vicinity of 300 µm in any direction. The olfactory bulbs of normal cases are exemplified by Case OFB48: the ventral surface features glomerular voxels densely and evenly, and the dorsal surface is relatively devoid of glomerular voxels. Case PD50 has a more even distribution of glomerular voxels in the dorsal versus ventral aspect, with the dorsal surface hosting several hotspots of high density. Case OFB43 also shows a bias to the ventral surface in terms of glomerular voxel density, but is comparable along the anterior–posterior axis between the dorsal and ventral aspects. The coverage, density, and distribution of glomerular voxels vary greatly among cases with differing density, extent, and patterning.

Staining of pSer129 α-synuclein in olfactory bulbs of Parkinson's disease cases

To visualize aggregates in the form of Lewy bodies and Lewy neurites, we performed immunohistochemistry for α-synuclein phosphorylated at Ser129 (pSer129 α-synuclein), a pathological hallmark of Parkinson's disease (Spillantini *et al.*, 1997). We analysed four normal cases (Cases OFB42, OFB48, OFB58, and OFB59) and four Parkinson's disease cases (Cases PD30, PD50, PD52, and PD53). Because the normal cases were, as expected, virtually devoid of this pathological staining, we concentrated our analyses on the Parkinson's disease cases. We detected prominent pSer129 α-synuclein staining throughout the olfactory bulb of these Parkinson's disease cases (Fig. 7A). The highest concentration of staining was found in the anterior olfactory nucleus, with Case PD52 exhibiting dense Lewy bodies and Lewy neurites in the anterior olfactory nucleus (Fig. 7B). High magnification analysis revealed frequent instances of what appear to be periglomerular neurons exhibiting varying degrees of pSer129 α-synuclein staining (Fig. 7C–I). We asked if a similar relationship as we had observed between the depth profiles of TH+ voxels and glomerular voxels also existed for pSer129 α-synuclein+ voxels and glomerular voxels. Here we masked out the anterior olfactory nucleus because its pSer129 α-synuclein load would massively skew the comparison of pSer129 α-synuclein+ voxels versus glomerular voxels. We thus restricted our analysis to the olfactory bulb minus the anterior olfactory nucleus, with the posterior boundary defined by the extent at which the last glomerulus could be observed. Examining the plots of pSer129 α-synuclein+ voxels along the depth dimension (Fig. 7J), we observed a significant direct correlation (Pearson correlation: Case PD53, $r = 0.6648$, $P = 0.0256$, $R^2 = 0.4420$; Case PD50, $r = 0.8295$, $P = 0.0016$, $R^2 = 0.6881$; Case PD30, $r = 0.7951$, $P = 0.0034$, $R^2 = 0.6321$; Case PD52, $r = 0.6055$, $P = 0.0484$, $R^2 = 0.3666$). Plotting the proportion of pSer129 α-synuclein+ voxels (the pSer129 α-synuclein load) versus the GGVV showed an inverse correlation: the higher the pSer129 α-synuclein load, the lower the GGVV, with a coefficient of determination of $R^2 = 0.99935$ to a logarithmic relationship (Fig. 7K).

Discussion

Glomeruli in the olfactory bulb of human versus mouse

Comparative analysis of the glomerular array in the olfactory bulbs from normal and Parkinson's disease cases revealed a substantial degree of variability, as is true for most qualitative and quantitative characteristics of olfactory bulbs from normal cases. The gross morphology of the olfactory bulbs varied in shape and size, and an irregular shape of the bulb was observed more consistently in Parkinson's disease cases. We confirm that the thousands of glomeruli in the human olfactory bulb lack the organized, uniform, and spherical morphology typical for mouse glomeruli, but exhibit a broad range of shapes and sizes, in normal and Parkinson's disease cases. Obviously there are major differences between mouse and human other than size, such as in genetic diversity, environment, lifestyle, and lifespan. Mouse studies are typically done in mice of inbred strains; in mice that are born and housed in ventilated cages; in mice that grow up and live in specified pathogen-free conditions; in mice that are subjected to a restricted and largely constant olfactory environment. Mice rarely get older than 2 years. In contrast, humans are outbred; they are raised in the 'wild'; they experience a much broader range of olfactory stimuli including noxious stimuli that may cause cell death and subsequent regeneration; and they suffer from numerous episodes of rhinitis over their lifespan of 80+ years due to the common cold. The human olfactory bulbs that are donated for research purposes typically come from aged individuals. The occurrence of invasive or atypical glomeruli in human olfactory bulbs is among the most pronounced differences compared with the mouse, and has been reported previously (Hoogland *et al.*, 2003; Maresh

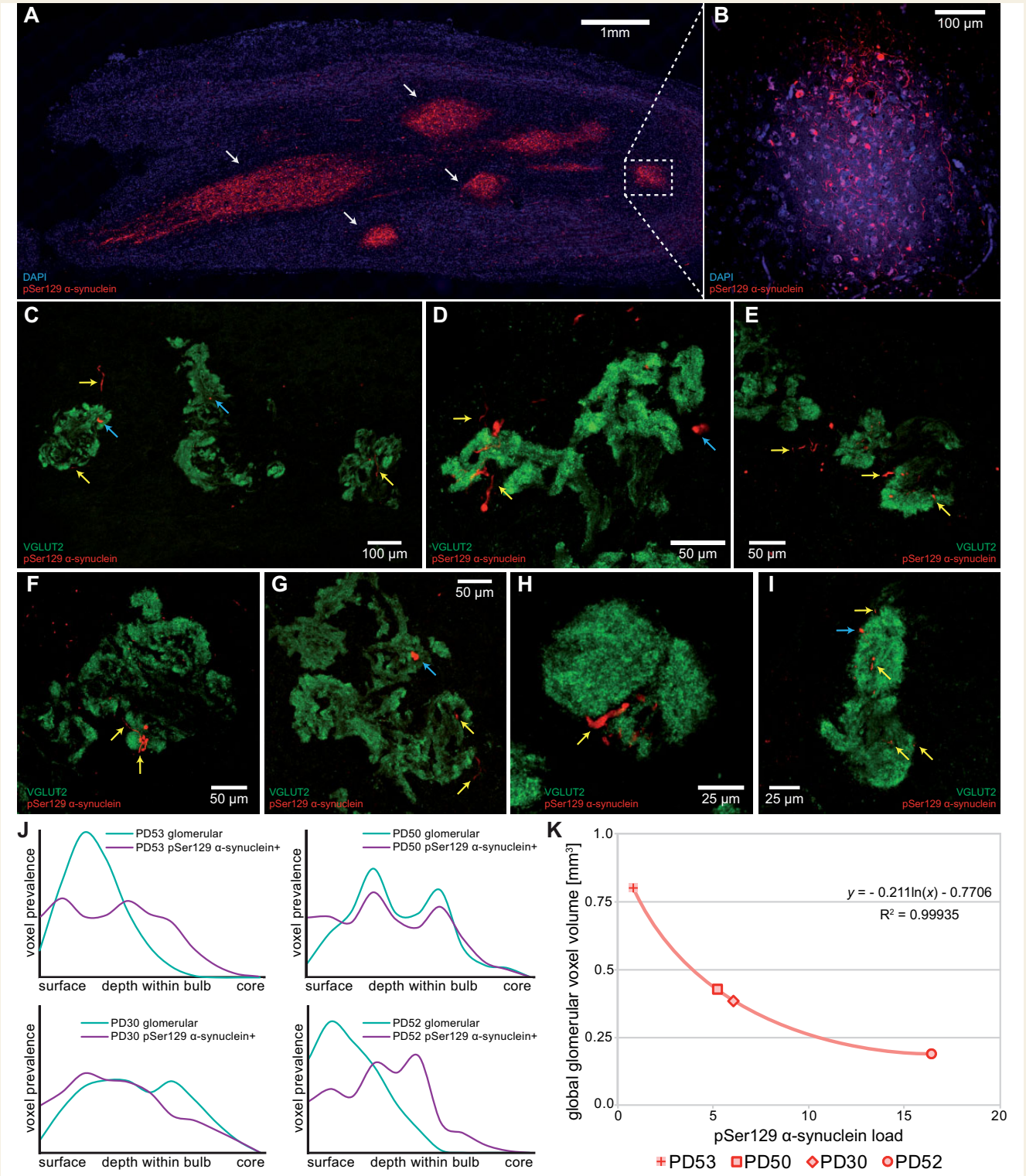

Figure 7 Phosphorylated Ser129 α-synuclein staining in Parkinson's disease cases. (**A**) Low-magnification fluorescence image of a horizontal section from Parkinson's disease Case PD52 stained with antibodies for VGLUT2 and phosphorylated α-synuclein (pSer129 α-synuclein). This case exhibits a heavy pSer129 α-synuclein load in the anterior olfactory nucleus (arrows), and moderate pSer129 α-synuclein staining surrounding glomeruli. (**B**) High-magnification image of a part of the anterior olfactory nucleus corresponding to the highlighted box in (**A**) rotated ~90° clockwise displaying prominent pSer129 α-synuclein staining of Lewy neurites and Lewy bodies. (**C–I**) High-magnification images of pSer129 α-synuclein staining in the form of Lewy bodies (blue arrows) and Lewy neurites (yellow arrows) within and surrounding glomeruli. Case PD50 (**C–G**), Case PD30 (**H** and **I**). (**J**) Depth profile of pSer129 α-synuclein + voxels in four Parkinson's disease cases. (**K**) Graph plotting pSer129 α-synuclein load versus GGVV in four Parkinson's disease cases. The pSer129 α-synuclein load encompasses the entire olfactory bulb except for the anterior olfactory nucleus, which was masked out from this analysis. The *x*-axis given in μm^3 of pSer129 α-synuclein + voxels per 1000 μm^3 of olfactory bulb.

et al., 2008). Such glomeruli may be a normal characteristic of the human olfactory bulb throughout life, or the cumulative result of insults and imperfections collected over a lifetime of decades.

Global glomerular voxel volume instead of counts of glomeruli

We believe that, for now, counts of glomeruli in human olfactory bulbs are not so informative and may even be misleading. First and foremost, it has proved difficult to identify individual glomeruli unambiguously in sections or in 3D reconstructions, given their irregular shapes and sizes. Second, even if there were an objective method to count glomeruli unambiguously and reproducibly, a basic understanding of what a human olfactory bulb glomerulus represents is still missing. It would be tempting to speculate that, by analogy to mouse (Mombaerts *et al.*, 1996; Treloar *et al.*, 2002), a human olfactory bulb glomerulus is formed and exclusively innervated by the coalescence of axons from OSNs expressing the same odorant receptor. But to date there is no evidence for this fundamental organizational principle of wiring in human, or in non-human primates. With ~400 odorant receptor genes in the human genome (Malnic *et al.*, 2004) and 2975 to 9325 glomeruli in the human olfactory bulb (Maresh *et al.*, 2008), the ratio of two to three glomeruli per odorant receptor gene observed in mouse does not extend to humans, where the ratio is 7 to 23 (Maresh *et al.*, 2008). This quantitative difference of as much as one order of magnitude in ratio between mouse and human may reflect a profound qualitative difference in wiring logic, which remains to be discovered. It is within the realm of possibility that a human olfactory bulb glomerulus is co-innervated by axons of multiple populations of OSNs each expressing a different odorant receptor or perhaps even multiple odorant receptors. Conversely, a population of human OSNs expressing a given odorant receptor may project their axons to multiple glomeruli. If the principle of homogeneity of glomerular innervation by OSN axons in terms of the expressed odorant receptor (Treloar *et al.*, 2002) holds true in humans, the next question is then whether the multiple glomeruli corresponding to a given odorant receptor are clustered or scattered in the human olfactory bulb. Until we understand what a human olfactory bulb glomerulus represents, it is prudent not to rely on counts of glomeruli for making inferences about mechanisms of olfactory coding in normal cases and of olfactory dysfunction in Parkinson's disease. Moreover, mere counts of glomeruli do not take into account their great variability in size.

Although we performed a software-based segmentation to automatically identify glomeruli on the basis of connected voxels, we refrained from counting glomeruli because our parameters affected the results of the counts. Instead we defined a novel and objective parameter—glomerular voxels with a resolution of ~10 μm^3—and computed the GGVV for a given olfactory bulb. When modelling glomeruli as perfect spheres with a diameter of ~60 µm, the GGVVs that we calculated here translate into a predicted range from 1630 to 10 807 glomeruli, which overlaps with the estimates of Maresh *et al.* (2008). We have previously shown in gene-targeted mouse strains that the total volume of the glomeruli corresponding to a given odorant receptor correlates very well with the number of OSNs that express this odorant receptor (Bressel *et al.*, 2016). If this finding translates to humans and remains valid under pathological conditions, the GGVV would serve as a surrogate marker for the number of OSNs that project from the olfactory epithelium to the olfactory bulb.

Parkinson's disease as an α-synucleinopathy in the olfactory bulb

A large body of literature has described Lewy pathology and α-synucleinopathy in the human olfactory bulb (Daniel and Hawkes, 1992; Rey *et al.*, 2017). The classical Braak staging of Parkinson's disease posits that pathology initiates in the olfactory bulb (Braak *et al.*, 2003*a*, 2004). Olfactory bulb α-synucleinopathy has a high specificity and sensitivity for Lewy body disorders, and accurately predicts the presence of α-synucleinopathy in other brain regions (Beach *et al.*, 2009). This body of evidence is consistent with the olfactory vector hypothesis, which has been proposed over the years in various formulations (Braak *et al.*, 2003*b*; Hawkes *et al.*, 2007; Doty, 2008; Rey *et al.*, 2017).

We found that the GGVV of olfactory bulbs from Parkinson's disease cases is ~47% that of normal cases. The average ± standard deviation (SD) for the predicted glomeruli based on perfectly spherical structures with a diameter of ~60 µm would be 3494 ± 2189 for Parkinson's disease cases, and 7428 ± 3096 for normal cases. It remains to be seen whether this reduction in GGVV reflects a reduced number of glomeruli, or a combination of a decrease in glomerular size and a reduced number of glomeruli. Arguably such a drastic reduction in the glomerular component of the olfactory bulb could in and of itself explain the olfactory dysfunction that is seen in >90% of Parkinson's disease patients (Doty, 2012).

We have shown that olfactory bulbs from Parkinson's disease cases with a higher α-synuclein load have a smaller GGVV, suggesting a causal relationship between this load and the reduction of the glomerular component of the olfactory bulb. However, the accumulation of pSer129 α-synuclein as Lewy bodies and Lewy neurites need not be unequivocally pathogenic but can be protective (Parkkinen *et al.*, 2011). Alternatively, an aetiological factor causes independently an aggregation of misfolded forms of α-synuclein (histologically detectable as Lewy bodies and Lewy neurites) and a reduction of the GGVV (fewer glomeruli and/or smaller glomeruli.)

We have documented a predominantly ventral deficit in glomerular voxels in Parkinson's disease cases: comparing

the average distribution of glomerular voxels between normal and Parkinson's disease cases indicates a ~13% reduction in the dorsal aspect, and a ~71% reduction ventrally. In a study by Sengoku *et al.* (2008), the localization of pathological α-synuclein in Parkinson's disease olfactory bulbs was mostly peripheral in early stages, and also became located in the anterior olfactory nucleus in later stages. This shift from peripherally to centrally in the olfactory bulb with disease progression may reflect the direction of the spread of α-synucleinopathy, and is consistent with the olfactory vector hypothesis. Likewise, the ventral bias of the reduction in glomerular voxels could be interpreted as consistent with xenobiotics or other damaging agents entering the olfactory bulb from the nasal cavity, and causing fewer and/or smaller glomeruli in the region of the olfactory bulb that is closest to the nasal cavity. However, the disease duration in this set of Parkinson's disease cases ranged from 9 to 20 years (average 13.2 years), such that the pathology in the olfactory bulb observed post-mortem may no longer reflect what occurred in the early stages of the disease. In an alternative hypothesis, fundamentally different populations of OSNs may reside in the dorsal versus ventral regions of the human olfactory epithelium, as is the case in mouse (Bozza *et al.*, 2009) and macaque (Horowitz *et al.*, 2014), and project their axons to dorsal or ventral aspects of the olfactory bulb (Bozz *et al.*, 2009). Insults to or loss of OSNs preferentially in the ventral olfactory epithelium would then result in a predominantly ventral deficit of the glomerular component in the olfactory bulb of Parkinson's disease cases. Lewy body α-synucleinopathy has been documented in the olfactory mucosa of patients with Parkinson's disease (Saito *et al.*, 2016).

Conclusion

Here we have reported a rigorous, quantitative, voxel-based approach to describe the glomerular component of the human olfactory bulb in 3D reconstructions generated from immunostained horizontal 10 µm section series. A distinct strength of our approach is that it encompasses the whole olfactory bulb. We confirm and extend that the laminar organization of the olfactory bulb is much less well defined in humans compared to that of inbred laboratory mice reared in controlled environments. We calculated that olfactory bulbs from Parkinson's disease cases contain approximately half as many glomerular voxels as normal cases, suggesting fewer and/or smaller glomeruli. Instead of the ventral preponderance of glomerular voxels in normal cases, glomerular voxels are more evenly distributed along the dorsal-ventral dimension in Parkinson's disease cases, indicating a predominantly ventral deficit. The simplest interpretation of our observation of the higher the α-synuclein load, the lower the GGVV, is a causal relationship between α-synucleinopathy and reduction of the glomerular component of the olfactory bulb.

A look ahead

To make further progress in our mechanistic understanding of olfactory dysfunction in Parkinson's disease, the questions that beg answers are if a human olfactory bulb glomerulus is innervated homogeneously by axons of OSNs expressing the same odorant receptor, and how the 7–23 glomeruli per human odorant receptor gene are distributed in the olfactory bulb. The answers to these questions may be provided by immunohistochemistry of human olfactory bulb sections with antibodies against a human odorant receptor that have been validated in mouse (Low and Mombaerts, 2017). Next it will be critical to determine if there are fundamental qualitative differences in the patterns of OSN axonal innervation of glomeruli between normal and Parkinson's disease cases. Qualitative differences in the wiring logic would help explain mechanistically the olfactory dysfunction in Parkinson's disease, in addition to the quantitative difference: the predominantly ventral deficit in the glomerular component of the olfactory bulb.

Acknowledgement

The authors gratefully acknowledge Marika Eszes for her technical input.

Funding

P.M. thanks the Max Planck Society for generous financial support, and the Royal Society of New Zealand for a Julius von Haast Fellowship. S.T. thanks the Auckland Medical Research Foundation for a postgraduate scholarship. M.A.C, B.V.D. and R.L.M.F thank the Neuroresearch Charitable Trust for generous financial support. The authors thank the Neurological Foundation of New Zealand for support of the Neurological Foundation Douglas Human Brain Bank.

References

Adler CH, Beach TG. Neuropathological basis of nonmotor manifestations of Parkinson's disease. Mov Disord 2016; 31: 1114–19.

Ansari KA, Johnson A. Olfactory function in patients with Parkinson's disease. J Chronic Dis 1975; 29: 493–7.

Baker H. Unilateral, neonatal olfactory deprivation alters tyrosine hydroxylase expression but not aromatic amino acid decarboxylase or GABA immunoreactivity. Neuroscience 1990; 36: 761–71.

Baker H, Kawano T, Margolis FL, Joh TH. Transneuronal regulation of tyrosine hydroxylase expression in olfactory bulb of mouse and rat. J Neurosci 1983; 3: 69–78.

Beach TG, White CL, Hladik CL, Sabbagh MN, Connor DJ, Shill HA, et al. Olfactory bulb α-synucleinopathy has high specificity and sensitivity for Lewy body disorders. Acta Neuropathol 2009; 117: 169–74.

Bozza T, Vassalli A, Fuss S, Zhang JJ, Weiland B, Pacifico R, et al. Mapping of class I and class II odorant receptors to glomerular domains by two distinct types of olfactory sensory neurons in the mouse. Neuron 2009; 61: 220–33.

Braak H, Del Tredici K, Rüb U, de Vos RA, Jansen Steur EN, Braak E. Staging of brain pathology related to sporadic Parkinson's disease. Neurobiol Aging 2003a: 197–211.

Braak H, Rüb U, Gai WP, Del Tredici K. Idiopathic Parkinson's disease: possible routes by which vulnerable neuronal types may be subject to neuroinvasion by an unknown pathogen. J Neural Transm 2003b; 110: 517–36.

Braak H, Ghebremedhin E, Rüb U, Bratzke H, Del Tredici K. Stages in the development of Parkinson's disease-related pathology. Cell Tissue Res 2004; 318: 121–34.

Bressel OC, Khan M, Mombaerts P. Linear correlation between the number of olfactory sensory neurons expressing a given mouse odorant receptor gene and the total volume of the corresponding glomeruli in the olfactory bulb. J Comp Neurol 2016; 524: 199–209.

Carpenter AE, Jones TR, Lamprecht MR, Clarke C, Kang IH, Friman O, et al. CellProfiler: image analysis software for identifying and quantifying cell phenotypes. Genome Biol 2006; 7: R100.

Daniel SE, Hawkes CH. Preliminary diagnosis of Parkinson's disease by olfactory bulb pathology. Lancet 1992; 340: 186.

Del Tredici K, Rüb U, De Vos RA, Bohl JRE, Braak H. Where does parkinson disease pathology begin in the brain? J Neuropathol Exp Neurol 2002; 61: 413–26.

Doty RL. The olfactory vector hypothesis of neurodegenerative disease: is it viable? Ann Neurol 2008; 63: 7–15.

Doty RL. Olfactory dysfunction in Parkinson disease. Nat Rev Neurol 2012; 8: 329–39.

Doty RL, Deems DA, Stellar S. Olfactory dysfunction in parkinsonism: a general deficit unrelated to neurologic signs, disease stage, or disease duration. Neurology 1988; 38: 1237–44.

Fujiwara H, Hasegawa M, Dohmae N, Kawashima, A, Masliah E, Goldberg MS, et al. α-synuclein is phosphorylated in synucleinopathy lesions. Nat Cell Biol 2002; 4: 160–4.

Hawkes CH, Del Tredici K, Braak H. Parkinson's disease: a dual-hit hypothesis. Neuropathol Appl Neurobiol 2007: 33: 599–614.

Hoogland PV, van den Berg R, Huisman E. Misrouted olfactory fibres and ectopic olfactory glomeruli in normal humans and in Parkinson and Alzheimer patients. Neuropathol Appl Neurobiol 2003; 29: 303–11.

Horowitz LF, Saraiva LR, Kuang D, Yoon KH, Buck LB. Olfactory receptor patterning in a higher primate. J Neurosci 2014; 34: 12241–52.

Leopold DA, Hummel T, Schwob JE, Hong SC, Knecht M, Kobal G. Anterior distribution of human olfactory epithelium. Laryngoscope 2000; 110: 417–21.

Low VF, Mombaerts P. Odorant receptor proteins in the mouse main olfactory epithelium and olfactory bulb. Neuroscience 2017; 344: 167–77.

Malnic B, Godfrey PA, Buck LB. The human olfactory receptor gene family. Proc Natl Acad Sci USA 2004; 101: 2584–9.

Maresh A, Rodriguez Gil D, Whitman MC, Greer CA. Principles of glomerular organization in the human olfactory bulb – implications for odor processing. PLoS One 2008; 3: e2640.

Mombaerts P, Wang F, Dulac C, Chao SK, Nemes A, Mendelsohn M, et al. Visualizing an olfactory sensory map. Cell 1996; 87: 675–86.

Morrison EE, Costanzo RM. Morphology of the human olfactory epithelium. J Comp Neurol 1990; 297: 1–13.

Nakashima T, Kimmelman CP, Snow JB. Olfactory marker protein in the human olfactory pathway. Arch Otolaryngol 1985; 111: 294–7.

Parkkinen L, O'Sullivan SS, Collins C, Petrie A, Holton JL, Revesz T, et al. Disentangling the relationship between Lewy bodies and nigral neuronal loss in Parkinson's disease. J Parkinsons Dis 2011; 1: 277–86.

Rey NL, Wesson DW, Brundin P. The olfactory bulb as the entry site for prion-like propagation in neurodegenerative diseases. Neurobiol Dis 2017, in press. doi: 10.1016/j.nbd.2016.12.013.

Richard MB, Taylor SR, Greer CA. Age-induced disruption of selective olfactory bulb synaptic circuits. Proc Natl Acad Sci USA 2010; 107: 15613–18.

Saito Y, Shioya A, Sano T, Sumikura H, Murata M, Murayama S. Lewy body pathology involves the olfactory cells in Parkinson's disease and related disorders. Mov Disord 2016; 31: 135–8.

Saraiva LR, Ibarra-Soria X, Khan M, Omura M, Scialdone A, Mombaerts P, et al. Hierarchical deconstruction of mouse olfactory sensory neurons: from whole mucosa to single-cell RNA-seq. Sci Rep 2015; 5: 18178.

Sengoku R, Saito Y, Ikemura M, Hatsuta H, Sakiyama Y, Kanemaru K, et al. Incidence and extent of Lewy body-related α-synucleinopathy in aging human olfactory bulb. J Neuropathol Exp Neurol 2008; 67: 1072–83.

Smith RL, Baker H, Kolstad K, Spencer DD, Greer CA. Localization of tyrosine hydroxylase and olfactory marker protein immunoreactivities in the human and macaque olfactory bulb. Brain Res 1991; 548: 140–8.

Smith RL, Baker H, Greer CA. Immunohistochemical analyses of the human olfactory bulb. J Comp Neurol 1993; 333: 519–30.

Spillantini MG, Schmidt ML, Lee VM, Trojanowski JQ, Jakes R, Goedert M. α-Synuclein in Lewy bodies. Nature 1997; 388: 839–40.

Treloar HB, Feinstein P, Mombaerts P, Greer, CA. Specificity of glomerular targeting by olfactory sensory axons. J Neurosci 2002; 22: 2469–77.